

Article

Enhanced Electrostrictive Coefficient and Suppressive Hysteresis in Lead-Free $\text{Ba}_{(1-x)}\text{Sr}_x\text{TiO}_3$ Piezoelectric Ceramics with High Strain

Mu Song^{1,2,3} , Xiaoyuan Sun^{1,2,3}, Qiong Li^{1,2,3}, Hao Qian^{1,2,3}, Yunfei Liu^{1,2,3,*} and Yinong Lyu^{1,2,3,*}

- ¹ The State Key Laboratory of Materials-Oriented Chemical Engineering, College of Materials Science and Engineering, Nanjing Tech University, Nanjing 210009, China; 201861203103@njtech.edu.cn (M.S.); 201862103012@njtech.edu.cn (X.S.); 201961103056@njtech.edu.cn (Q.L.); 202010006720@njtech.edu.cn (H.Q.)
- ² Jiangsu National Synergetic Innovation Center for Advanced Materials (SICAM), Nanjing Tech University, Nanjing 210009, China
- ³ Jiangsu Collaborative Innovation Center for Advanced Inorganic Function Composites, Nanjing Tech University, Nanjing 210009, China
- * Correspondence: yfliu@njtech.edu.cn (Y.L.); yinonglu@njtech.edu.cn (Y.L.); Tel.: +86-25-8317-2118 (Y.L.); +86-25-8317-2120 (Y.L.)

Abstract: Lead-free piezoelectric ceramics with both low hysteresis and superior electrostrictive coefficient features are crucial toward providing desired performance for intelligent electrical devices, especially in high-precision displacement actuators. In this work, we propose a novel scenario, which is to design the phase transition around ambient temperature to enhance electrostrictive effect and inhibit hysteresis. In other words, the dense ceramics with cubic phases (C) and tetragonal phases (T) coexisting at RT (room temperature) were designed. According to this scenario, the $\text{Ba}_{(1-x)}\text{Sr}_x\text{TiO}_3$ (abbreviated as BT-100xST) ceramics were fabricated by the conventional solid-state reaction method. The relaxor behavior, ferroelectric properties, crystal structure and microstructure of BT-100xST ceramics have been investigated in detail. As a result, the BT-100xST ceramics with $x = 0.20\text{--}0.40$ present relaxor behavior which was indicated by dielectric constant as a function of temperature and (polarization–electric field) P – E hysteresis loops. The BT-30ST ceramics exhibit enhanced electrostrictive coefficient Q_{33} ($>0.034 \text{ m}^4/\text{C}^2$), and the electrostrictive strain and low hysteresis achieves 0.11% and 2%, respectively. The BT-100xST ceramics are considered as a prospective option for application in displacement actuators with high sensitivity and high precision.

Keywords: barium strontium titanate; crystal structure; hysteresis; electrostrictive coefficient



Citation: Song, M.; Sun, X.; Li, Q.; Qian, H.; Liu, Y.; Lyu, Y. Enhanced Electrostrictive Coefficient and Suppressive Hysteresis in Lead-Free $\text{Ba}_{(1-x)}\text{Sr}_x\text{TiO}_3$ Piezoelectric Ceramics with High Strain. *Crystals* **2021**, *11*, 555. <https://doi.org/10.3390/cryst11050555>

Academic Editors: Gilles Gauthier, Jong-Sook Lee, Sandrine Ricote and Sebastian Wachowski

Received: 16 April 2021

Accepted: 13 May 2021

Published: 16 May 2021

Publisher's Note: MDPI stays neutral with regard to jurisdictional claims in published maps and institutional affiliations.



Copyright: © 2021 by the authors. Licensee MDPI, Basel, Switzerland. This article is an open access article distributed under the terms and conditions of the Creative Commons Attribution (CC BY) license (<https://creativecommons.org/licenses/by/4.0/>).

1. Introduction

Piezoelectric ceramics have been widely used in electronic devices, such as sensors, actuators, and transducer and ultrasonic motors [1–3], which are required not only high-strain but also ultra-low hysteresis. However, many researchers just devoted themselves to realizing the critical target of achieving large electric-field-induced strain. Hao et al. [4,5] fabricated high-strain ceramics by designing a phase transition from a ferroelectric to an ergodic relaxor phase in the lead-free ternary $\text{Bi}_{0.5}\text{Na}_{0.4}\text{K}_{0.1}\text{TiO}_3\text{--K}_x\text{Na}_{1-x}\text{NbO}_3$ systems. In this scenario, however, a high-strain response is commonly accompanied by large hysteresis $> 60\%$ with strong nonlinearity. Based on this strategy, other works also reported on $\text{Bi}_{0.5}\text{N}_{0.5}\text{TiO}_3$ -based ceramics, accompanying high hysteresis that is observed simultaneously [6,7]. Recently, several studies demonstrated the addition of compound or cation doping can suppress hysteresis [8,9]. For instance, relatively small hysteresis—as low as 23%—was achieved in a $\text{Bi}_4\text{Ti}_3\text{O}_{12}\text{--Bi}_{0.5}(\text{Na}_{0.82}\text{K}_{0.18})_{0.5}\text{TiO}_3$ system, as reported by Fan et al. [10], which is attributed to A-site vacancies to destroy the long-range ferroelectric order and promote the formation of the extremely stable relaxor phase at room temperature.

Another effective method to overcome the significant challenge of high hysteresis is to design relaxor ferroelectric with electrostrictive strain. For the canonical lead-free BNT-based relaxor, the electrostrictive strain refers to “a ferroelectric relaxor + a ferroelectric” for solid solutions [11]. However, the electrostrictive coefficient is low ($Q_{33} = 0.020\text{--}0.024 \text{ m}^4/\text{C}^2$) [12]. A large strain predominantly based on electrostrictive effect has been demonstrated in lead-based relaxor ferroelectrics with a T—C coexisting phase structure. Meanwhile, researchers found that doping enhanced the dielectric diffuseness and relaxation and inhibited hysteresis. As an important figure of merit, the Q_{33} in PMN-based systems, including $\text{PbMg}_{1/3}\text{Nb}_{2/3}\text{O}_3\text{-PbTiO}_3$ [13], $\text{Pb}(\text{In}_{1/2}\text{Nb}_{1/2})\text{O}_3\text{-Pb}(\text{Mg}_{1/3}\text{Nb}_{2/3})\text{O}_3\text{-PbTiO}_3$ [14], $\text{Bi}(\text{Li}_{0.5}\text{Nb}_{0.5})\text{O}_3\text{-Pb}(\text{Mg}_{1/3}\text{Nb}_{2/3})\text{O}_3\text{-PbTiO}_3$ [15], etc., ranges from $0.03 \text{ m}^4/\text{C}^2$ to $0.04 \text{ m}^4/\text{C}^2$. A high strain of 0.16–0.20% with low hysteresis < 7% was also observed in these samples. However, in today’s environmentally conscious world, lead-free electrostrictive materials are highly desirable for safety reasons because of the toxicity of lead compounds [16,17].

BaTiO_3 -based ferroelectric ceramics are one of the most promising lead-free replacements, owing to the relatively high electric field strain and low hysteresis compared with other systems of piezoelectric ceramics. These superior strain properties come from remarkable piezoelectric effects around the polymorphic phase boundary (PPB) or morphological phase boundary (MPB) [18]. Wu et al. reported that the addition of Sr^{2+} is a modifier that could effectively shift the $T_{\text{R-O}}$ (Rhombohedral—Orthorhombic) and $T_{\text{O-T}}$ (Orthorhombic—Tetragonal) values to construct phase boundary; as a result, 0.13% strain with 10% hysteresis was achieved [19]. Zhao et al. [20] explored a high-strain BT-based system of $(\text{Ba}_{1-y}\text{Ca}_y)(\text{Ti}_{1-x}\text{Hf}_x)\text{O}_3$, which had the surprisingly enormous strain of $S_{\text{max}} = 0.21\%$ and piezoelectricity coefficient of $d_{33} = 540 \text{ pC/N}$ by constructing multiphase coexistence, including the R, O and T. Nevertheless, these samples were accompanied by hysteresis > 10%. It can be expected that we can possibly design BT-based piezoelectric ceramics of electrostrictive effect near the phase boundary, which exhibit high-strain ceramics and further suppress hysteresis.

Following the above research, we designed lead-free BaTiO_3 -based system piezoelectric ceramics by doping a cubic SrTiO_3 into tetragonal BaTiO_3 [21]. The two crystal structures of cubic and tetragonal were selected as a result of both having the potential to form a ferroelectric and paraelectric phase boundary. At this time, the strain of BT-100xST piezoelectric ceramics were generated by electrostrictive effect [22]. Meanwhile, the BT-ST solid solution was confirmed because equivalent substitution can induce relaxor ferroelectric with low hysteresis [23]. In the case of BT-100xST ceramics, although microwave-tunability [24], sintering behavior [25,26], and energy storage properties [27,28] have been researched extensively during the past decades, hysteresis and electrostrictive effects are still rarely reported. In the following, we shall expound the effect of Sr^{2+} addition to BaTiO_3 ceramics on the crystal structure, microstructure dielectric, ferroelectric, strain and electrostrictive properties. Consequently, we have achieved an extraordinary combination of low hysteresis, enhanced electrostrictive coefficient and high strain.

2. Materials and Methods

The powders of BaCO_3 (99.0%), SrCO_3 (99.0%), TiO_2 (99.0%) were weighted as starting raw materials according to the stoichiometric ratio of $\text{Ba}_{(1-x)}\text{Sr}_x\text{TiO}_3$ ($x = 0.10, 0.15, 0.20, 0.30, 0.40, 0.50$ and 0.60 , abbreviated as BT-100xST). The BT-100xST ceramics were fabricated by the conventional solid-state reaction method, and the preparation process mainly carried out the following chemical reactions to form a solid solution [24]. Details of the production process can refer to Refs. [29,30].



X-ray diffraction (XRD, Smart Lab 3 kW, Rigaku, Japan) analysis using Cu $K\alpha_1$ radiation was used to investigate the crystal structures of BT-100 x ST ceramics. The surface appearance of thermally-etched samples was imaged by scanning electron microscopy (SEM, JSM-6510, JEOL, Tokyo, Japan). A ferroelectric tester instrument (Precision Premier II, Radiant Technology, San Diego, CA, USA) was used to measure electric properties at room temperature, including bipolar polarization–electric field (P – E) hysteresis loops, bipolar and unipolar strain–electric field (S – E) curves and current–electric field (I – E) curves. Temperature-dependent dielectric permittivity and loss tangent under different frequencies (0.1 kHz, 1 kHz, 10 kHz, 100 kHz) were measured by an LCR (Lenz Capacitor Resistance) meter (4284 Agilent, Palo Alto, CA, USA) from -100 °C to 150 °C at a heating rate of 2 °C/min.

3. Results and Discussions

3.1. Microstructure

The room temperature XRD patterns of BT-100 x ST ceramics are illustrated in Figure 1a. It can be seen that the detectable peaks of all samples demonstrate a pristine perovskite structure without the presence of impurity peaks, implying that the Sr element has diffused into the BT lattice to form complete, solid solutions. The diffraction peaks shift steadily to higher angles with the increase in x (Figure 1b) as a result of the small radius (1.440 Å) Sr^{2+} substituting for the large radius (1.610 Å) Ba^{2+} , which in turn results in the crystal lattice shrinkage. Meanwhile, the diffraction peaks near 45° at $x < 0.40$ exhibit split characteristics, and show a tendency to merge with the increasing quantity of x . A single diffraction peak was observed in the composition with $x \geq 0.40$. To intuitively confirm the revolution of phase structure, all the peaks around 45° were depicted by peak fitting, as shown in Figure 1c. The sharp $(200)_T$, $(002)_T$ peaks and ultra-weaker $(200)_C$ peaks were identified in $x < 0.30$, which are attributed to a main tetragonal phase and infinitesimal cubic phase, while an obvious $(200)_C$ peak was detected for $x = 0.30$, indicating the coexistence of the T and C phase. With a further increase in x , the sharp $(200)_C$ peak and negligible $(002)_T$ peak were presented, suggesting the cubic phase nature of crystal structure.

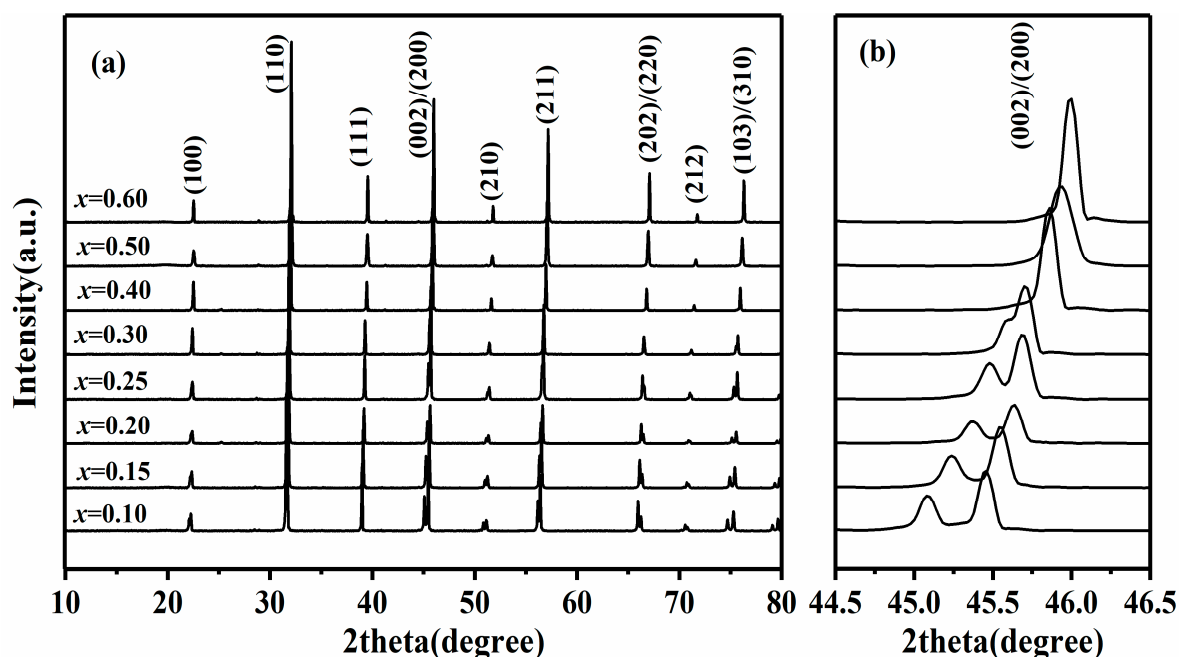


Figure 1. Cont.

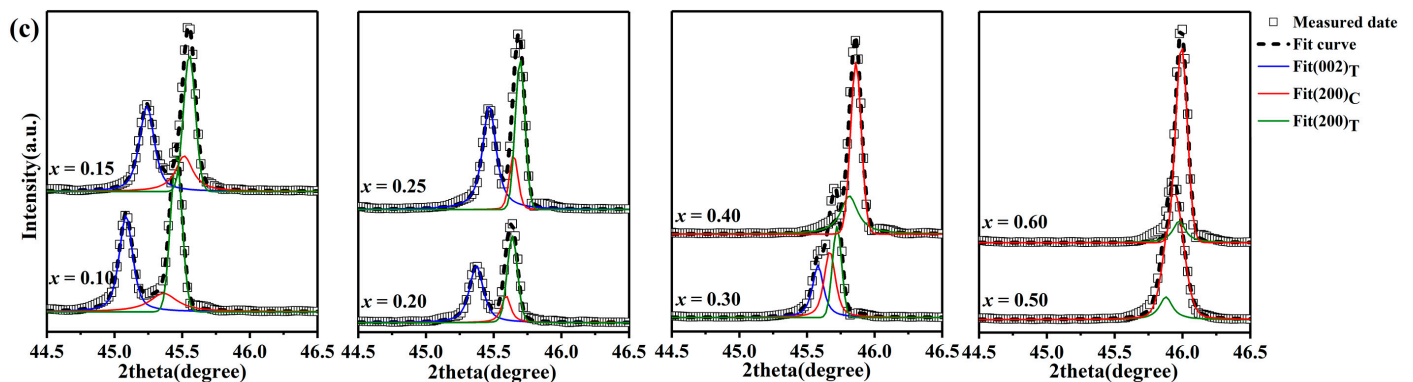


Figure 1. The X-ray diffraction (XRD) patterns of BT-100 x ST ($x = 0.10$ – 0.60) ceramics in the 2θ range of (a) 10 – 80° and (b) 44.5 – 46.5° , (c) peak fitting in the 2θ range of 44.35 – 46.25° .

The SEM surface images of the BT-100 x ST ceramics with different Sr contents are shown in Figure 2. All samples excellently exhibited dense grain structure, and the microstructures become uniform with the increasing of x . The average grain size of BT-100 x ST ceramics was obtained based on the statistical method and the corresponding results are illustrated in the inset of the SEM surface images. It is noted that the BT-10ST ceramics exhibit a large average grain size of $17.8 \mu\text{m}$, with the grain size gradually decreasing as a result of increased ST concentration. Eventually, the grain size decreases to $5.2 \mu\text{m}$ for BT-60ST ceramics. Above all, results imply that the Sr^{2+} ions can inhibit the growth of grains and lead to uniform micromorphology.

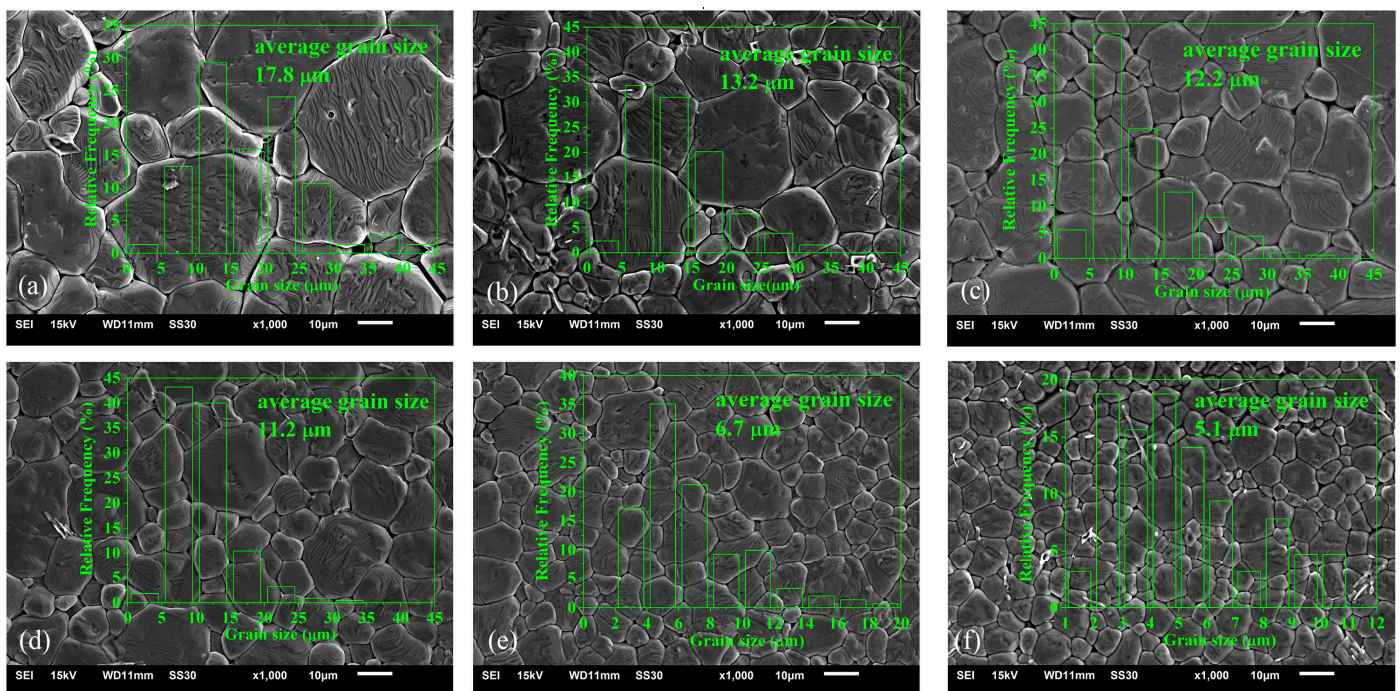


Figure 2. The scanning electron microscopy (SEM) images and average grain size (the inset corresponding to the SEM surface images) of BT-100 x ST ceramics, (a) $x = 0.10$, (b) $x = 0.15$, (c) $x = 0.20$, (d) $x = 0.30$, (e) $x = 0.40$, (f) $x = 0.50$, (g) $x = 0.60$.

3.2. Dielectric Behaviors

The phase structure of BT-100 x ST ceramics was further demonstrated by the temperature dependence of permittivity and loss tangent, as is presented in Figure 3a–g. It can be seen that several dielectric peaks and dielectric loss peaks associated with phase transition are detected, and they are denoted as T_m , T_1 , and T_2 . Following the decreasing

of temperature, T_m , T_1 , and T_2 correspond to the phase transition temperature of cubic paraelectric to tetragonal ferroelectric, tetragonal ferroelectric to orthorhombic ferroelectric, and orthorhombic ferroelectric to rhombohedral ferroelectric, respectively [31]. Increasing the ST content causes T_m , T_1 and T_2 to shift to low temperatures. In addition, the dielectric loss does not exceed 2% at higher frequencies. Note that the value of dielectric loss measured at 0.1 kHz rises dramatically when the temperature exceeds 80 °C. This might be due to charges or defects being activated easily at high temperature and low frequency [32]. According to the profile of permittivity and dielectric loss as a function of temperature, the phase diagram is depicted as shown in Figure 2h. The phase structure of BT-100xST ceramics is tetragonal for $x \leq 0.20$ and cubic for $x \geq 0.40$. For $x = 0.30$, the BT-30ST ceramics exhibit a tetragonal phase coexisting with the cubic phase at room temperature. This result is consistent with the phase structure determined by the XRD pattern.

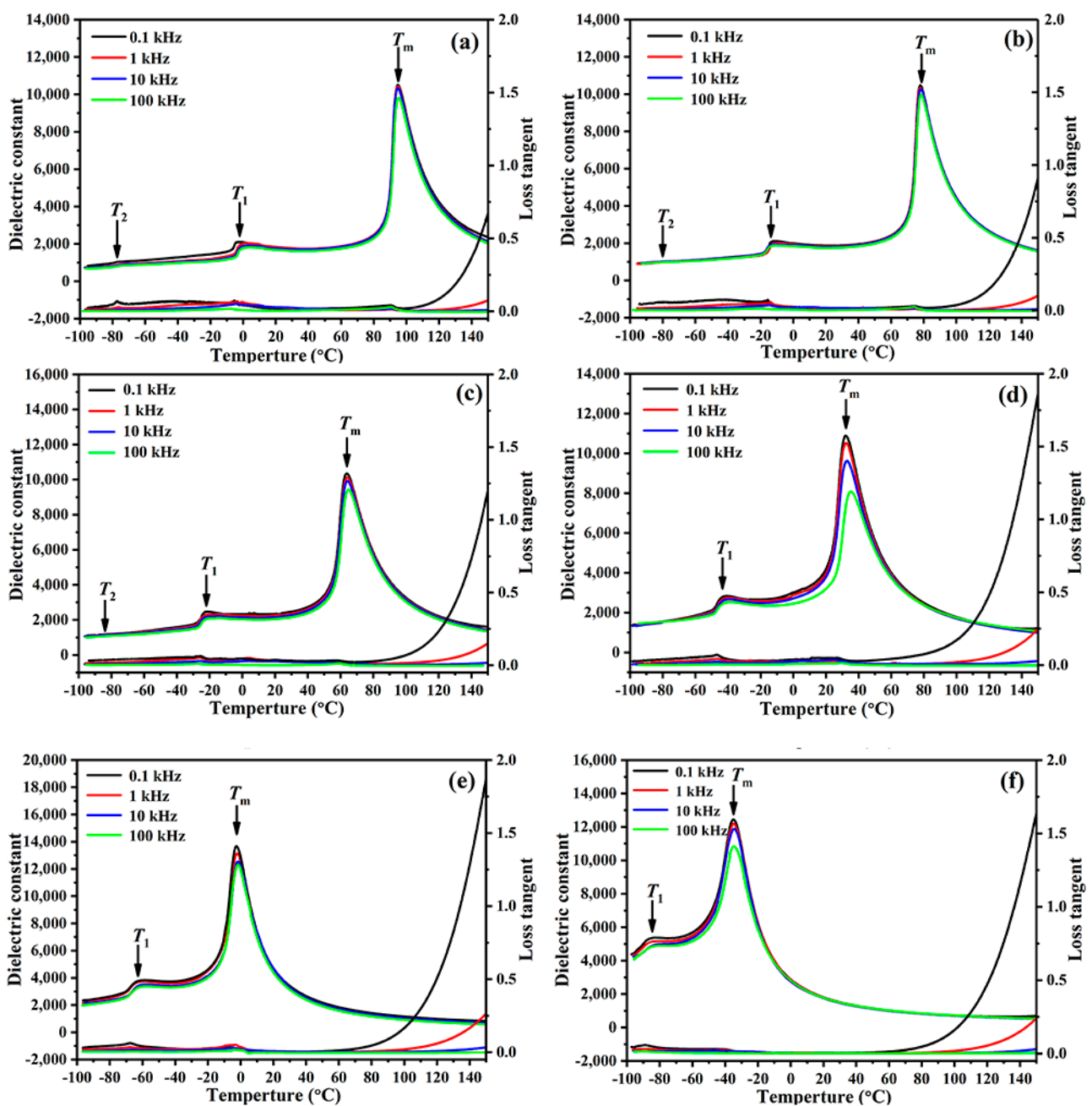


Figure 3. Cont.

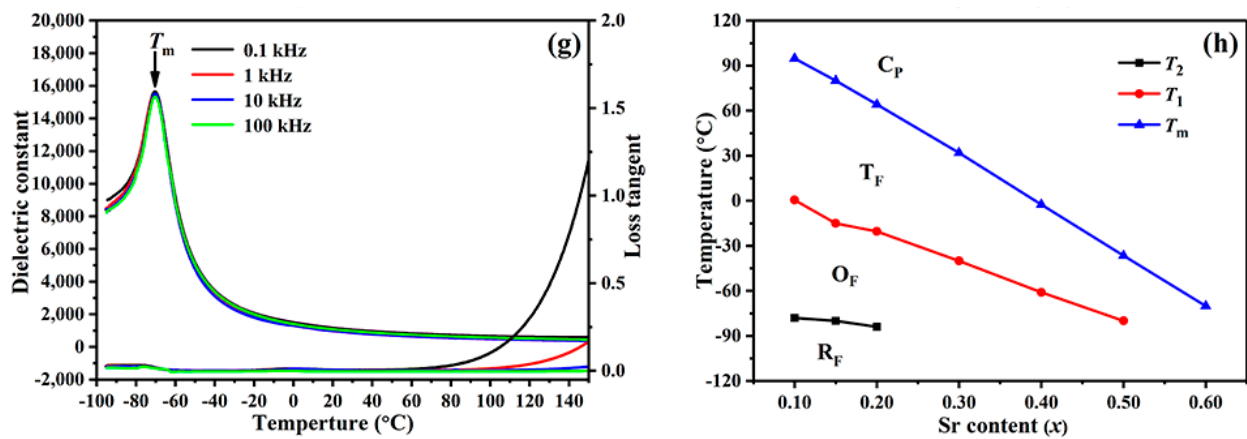


Figure 3. Temperature dependence of permittivity and loss tangent for BT-100xST, (a) $x = 0.10$, (b) $x = 0.15$, (c) $x = 0.20$, (d) $x = 0.30$, (e) $x = 0.40$, (f) $x = 0.50$, (g) $x = 0.60$ and (h) the phase diagram of BT-100xST based on T_m , T_1 and T_2 .

The further detail regarding the frequency dependence of permittivity as a function of temperature is presented in Figure 4. By increasing Sr content, the dielectric peaks begin flattening. Furthermore, the significant frequency dispersion that causes the dielectric constant to decline and the corresponding T_m peak shifts to increase in temperature at a higher frequency were observed at $x = 0.20$ – 0.40 . For x being up to 0.40, the dielectric anomaly peak becomes even narrower, which implies the feebleness of the relaxor degree. In general, a broad T_m peak exists in the composition of BT-100xST ceramics due to the diffuse phase transition (DPT).

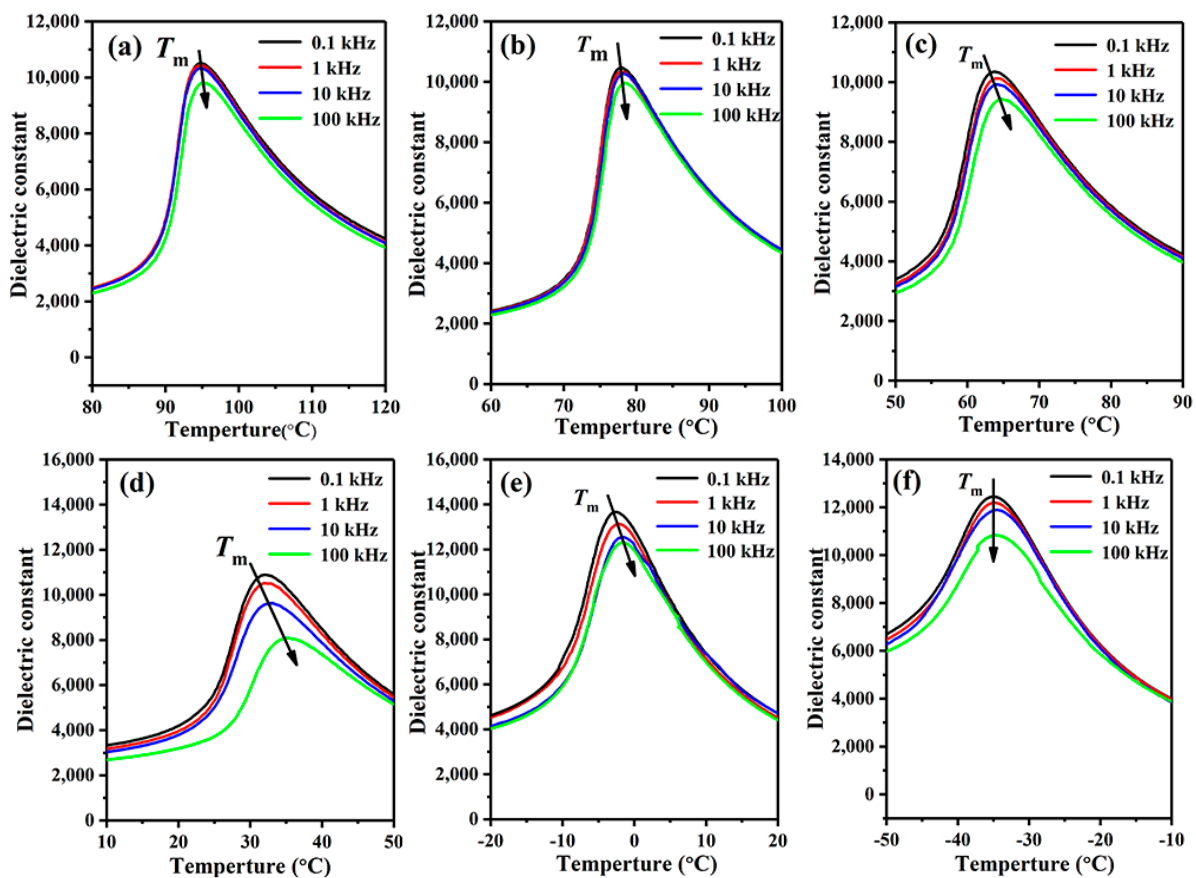


Figure 4. Cont.

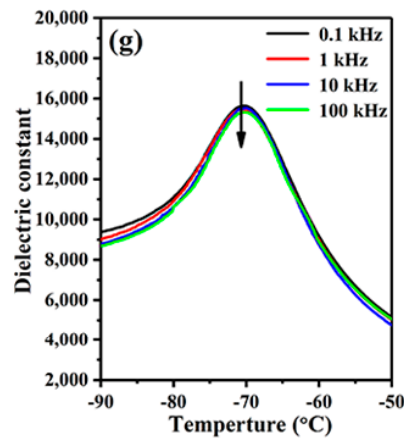


Figure 4. The frequency dependence of permittivity as a function of temperature for BT-100xST, (a) $x = 0.10$, (b) $x = 0.15$, (c) $x = 0.20$, (d) $x = 0.30$, (e) $x = 0.40$, (f) $x = 0.50$, (g) $x = 0.60$.

In order to analyze the diffuseness of the DPT quantitatively, a modified Curie–Weiss law is defined, followed by Equation (4) [33,34].

$$\frac{1}{\varepsilon} - \frac{1}{\varepsilon_r} = \frac{(T - T_m)^\gamma}{C} \quad (T > T_m) \quad (4)$$

where C is the Curie-like constant. The index γ represents the character of the phase transition; $\gamma = 1$ and $\gamma = 2$ correspond to a typical ferroelectric and absolute diffuse phase transition, respectively. For different compositions, the slope of a linear relation between $\ln(1/\varepsilon_r - 1/\varepsilon_m)$ and $\ln(T - T_m)$ was extracted by fitting a straight-line equation, as shown in Figure 5. With an increase in x from 0.10 to 0.30, the index γ value rises from 1.19 to 1.36, and then γ decreases to 1.10, where $x = 0.60$. The value of γ for $x = 0.30$ and 0.40 are 1.36 and 1.29, respectively. These results suggest that BT-30ST and BT-40ST ceramics have more obvious diffuse phase transitions, which corresponds to broader dielectric peaks. The fluctuation of local components leads to the occurrence of DPT, which leads to microregions with different local Curie points exhibiting a Gaussian distribution near the mean Curie temperature [35]. Above all, these results demonstrate that the ceramics with $x = 0.20$ –0.40 have canonical relaxor behavioral properties.

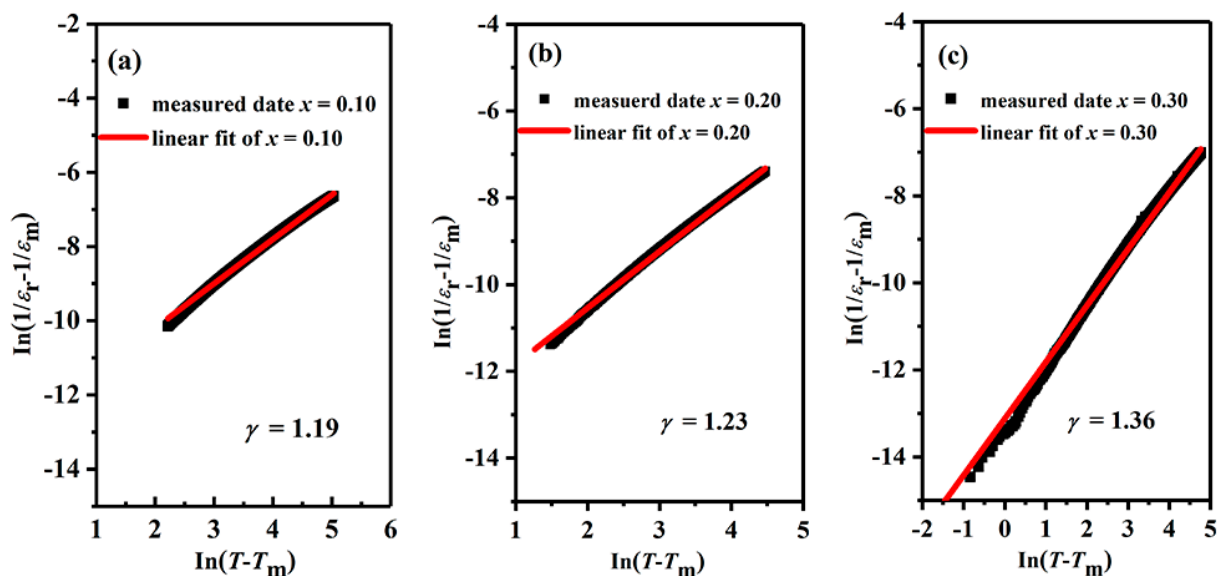


Figure 5. Cont.

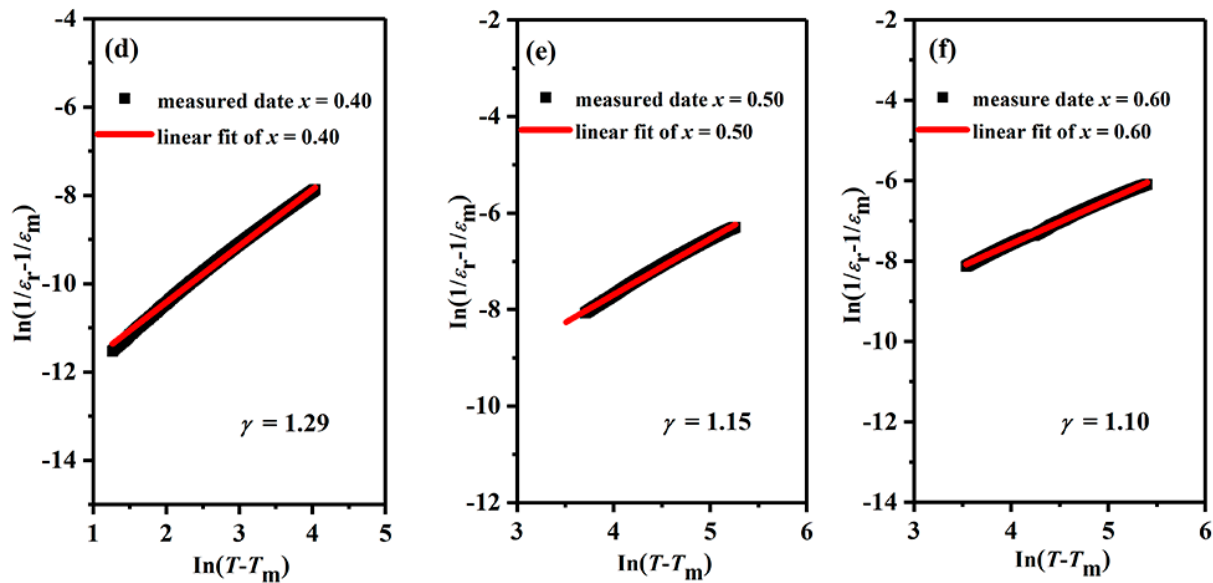


Figure 5. Linear fit graph of diffuseness factor γ of BT-100xST ceramics, (a) $x = 0.10$, (b) $x = 0.20$, (c) $x = 0.30$, (d) $x = 0.40$, (e) $x = 0.50$, (f) $x = 0.60$.

3.3. Ferroelectric and Piezoelectric Properties

Figure 6a presents the room temperature P - E hysteresis loops of BT-100xST ($x = 0.10$ – 0.60). The well-saturated hysteresis loops of low-doping BT-based ceramics ($x \leq 0.20$) are on the verge of typical ferroelectric behavior [36], and the high values of P_{\max} , P_r , and E_c were measured, corresponding to $26.2 \mu\text{C}/\text{cm}^2$, $14.1 \mu\text{C}/\text{cm}^2$ and $10.3 \text{ kV}/\text{cm}$, respectively, at $x = 0.10$. In the composition of $x = 0.10$ – 0.40 , it is worth noting that the hysteresis loop transformed from a square profile into a slim profile with the increase in x . The slim hysteresis loop implies the prominent relaxor characteristic. The variation of maximum polarization (P_{\max}), remnant polarization (P_r), and coercive electric field (E_c) as a function of x is depicted in Figure 6b. The decline of P_r and E_c is more dramatic than P_{\max} . As a result, the following values were achieved at $x = 0.40$: $P_r = 0.85 \mu\text{C}/\text{cm}^2$, $E_c = 1.5 \text{ kV}/\text{cm}$ and $P_{\max} = 16 \mu\text{C}/\text{cm}^2$. To better interpret the relaxor behavior, Figure 6c presents the I - E curves of BT-100xST ($x = 0.10$ – 0.60). For the ceramics with $x = 0.10$ – 0.40 , it is obviously observed that sharp current peaks gradually broaden. The broad current peaks also reflect a relaxor ferroelectric behavior of the ceramics with $x = 0.30$ – 0.40 [37]. The current peak is related to domain reversal, while a broad current peak refers to the switching of nano-domains, which is different from the sharp current peak generated by the switching of macro-domains [35]. With a further increase in ST content, the ceramic shows a linear feature, indicating that the BT-60ST ceramic is a linear dielectric material. It is worth noting that the corresponding I - E curves are a square loop. These results have also been reflected in other reports [38].

Figure 7 presents the room temperature S - E curves of BT-100xST ($x = 0.10$ – 0.60). The bipolar S - E curves (Figure 7a) show the butterfly-like shape at a low degree of substitution ($x \leq 0.20$), which exhibits the ferroelectric feature. In contrast, the S - E curves transform from the butterfly shape to a symmetric narrow shape (along with the disappearance of the negative electro-strain) as the x exceeds 0.30, originating from the appearance of typical relaxor ferroelectrics. The unipolar S - E curves (Figure 7b) show that the strain rises upward first and then falls down with the increasing value of x . The maximum value of unipolar strain was obtained in $x = 0.20$. Figure 7c clearly shows the variation of maximum strain (S_{\max}), negative strain (S_{neg}), and hysteresis (H_{ys}) as a function of x . For x being up to 0.20, the distinct negative strain is attributed to the irreversible ferroelectric domain wall switching [38]. Thereafter, it keeps a downward tendency and approximates to zero, suggesting that irreversible ferroelectric domains decrease. The strain hysteresis is defined by the equation: $H_{\text{ys}} = \Delta S / S_{\max} \times 100\%$, where ΔS is the difference of strain at a half

maximum field. The highest strain (0.20%) was obtained at $x = 0.20$, while accompanied by a relatively high hysteresis (11.48%). The superior property of less than 2% hysteresis with 0.11% strain was obtained at $x = 0.30$. With the further increase to $x = 0.50$, the hysteresis increases drastically.

3.4. Electrostrictive Effect

Compared with the extrinsic activity (domain wall motion) and piezoelectric effect, the electrostrictive contribution shows ultra-low hysteresis and high stability with response to the extra electric field [39,40]. The BT-30ST and BT-40ST ceramics present ultra-low hysteresis properties, which implies that the strain with the low hysteresis is mainly attributed to intrinsic electrostrictive effect rather than macro-domain switching. Figure 8 shows the strain as a function of polarization at room temperature of BT-100 x ST ceramics. The width trait of the S - P curves dependent of x also reflects the magnitude of the hysteresis as shown in S - E curves. According to the equation $S = QP^2$, Figure 9 shows the electrostriction coefficient Q_{33} obtained by the quadratic fitting of S and P derived from the corresponding S - E and P - E curves. The magnitude of the R coefficient of quadratic fitting S - P curves reflects the degree of deviation from the quadratic relation as shown in Figure 9. The value of R being distant from one means that the electrostrictive effect is reduced.

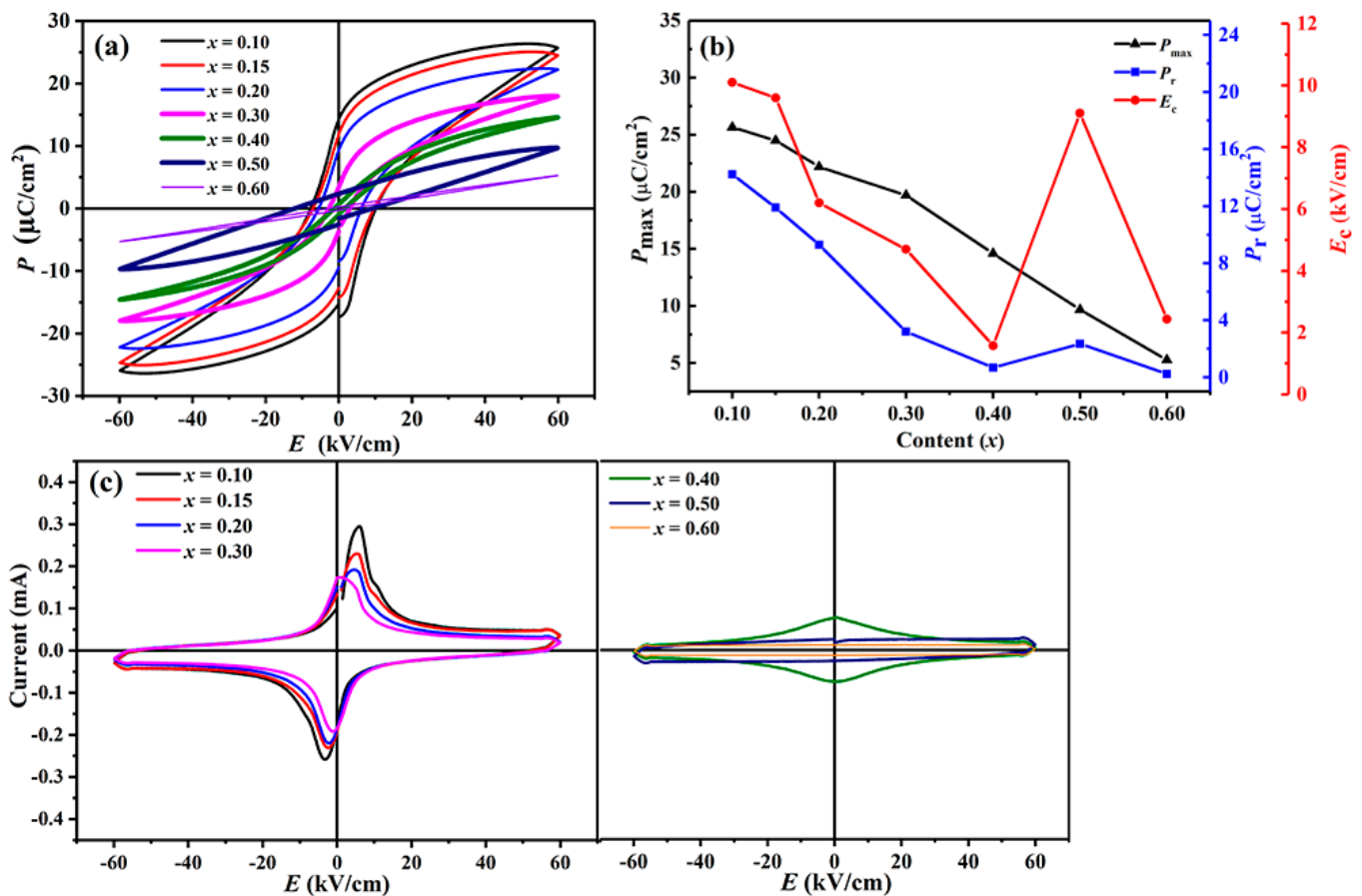


Figure 6. (a) P - E hysteresis loops of BT-100 x ST ceramics at room temperature, (b) the corresponding P_{max} , P_r and E_c of BT-100 x ST ceramics as a function of Sr contents, (c) the corresponding I - E curves.

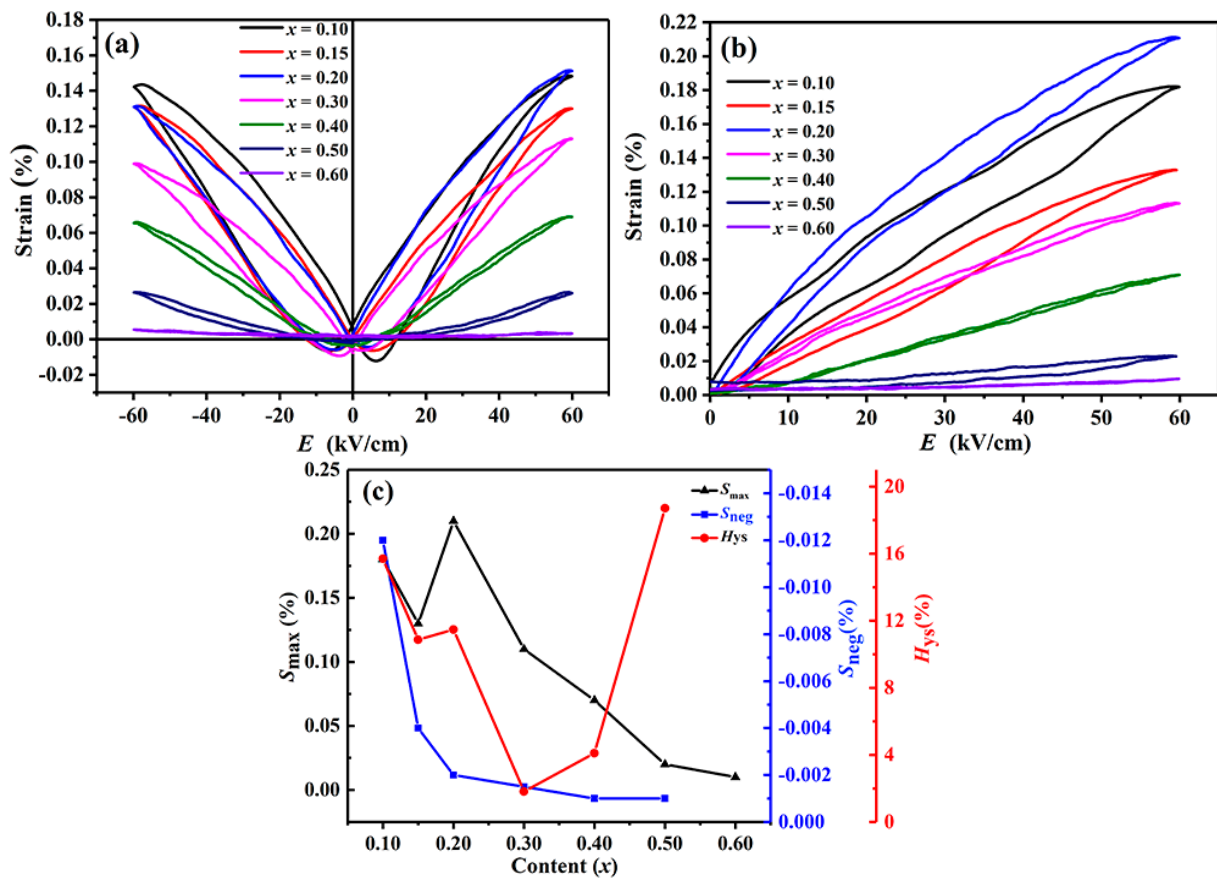


Figure 7. (a) Unipolar strain curves, (b) bipolar strain curves of BT-100xST ceramics with different Sr contents, (c) line chart of unipolar S_{max} , H_{ys} and S_{neg} .

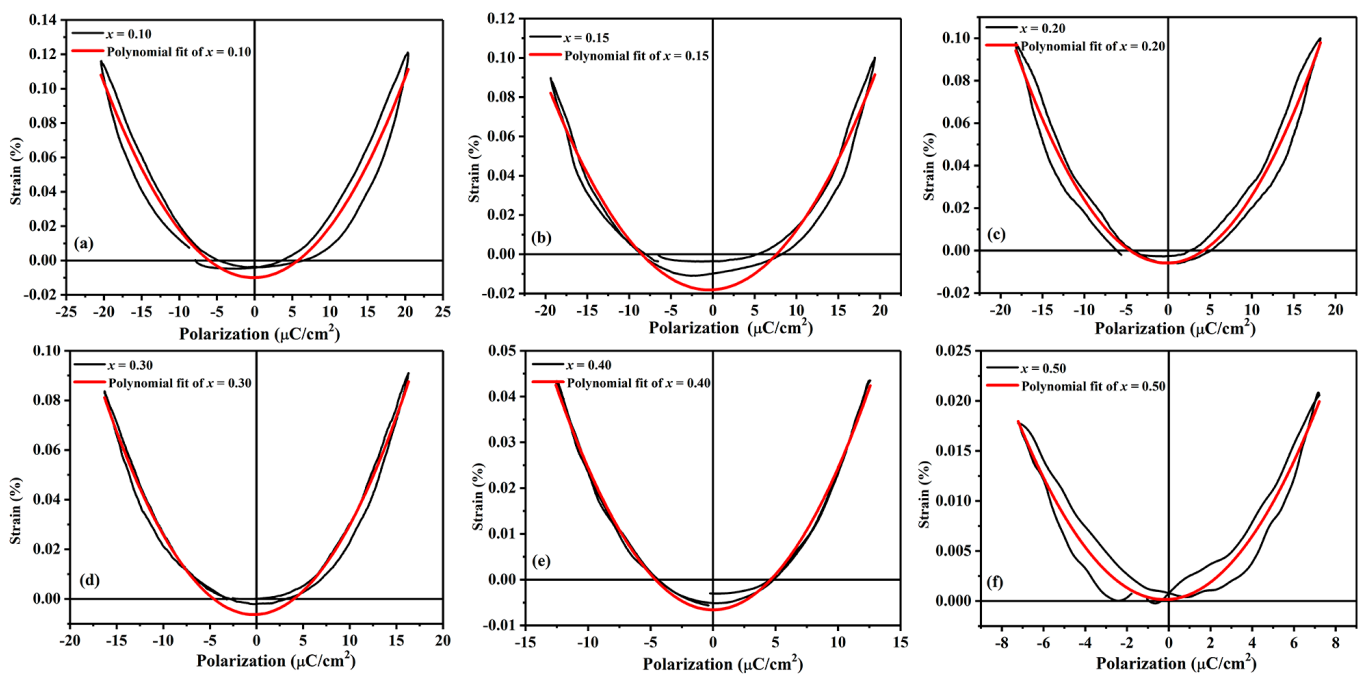


Figure 8. Bipolar S-P curves of BT-100xST ceramics with different Sr contents, (a) $x = 0.10$, (b) $x = 0.15$, (c) $x = 0.20$, (d) $x = 0.30$, (e) $x = 0.40$, (f) $x = 0.50$.

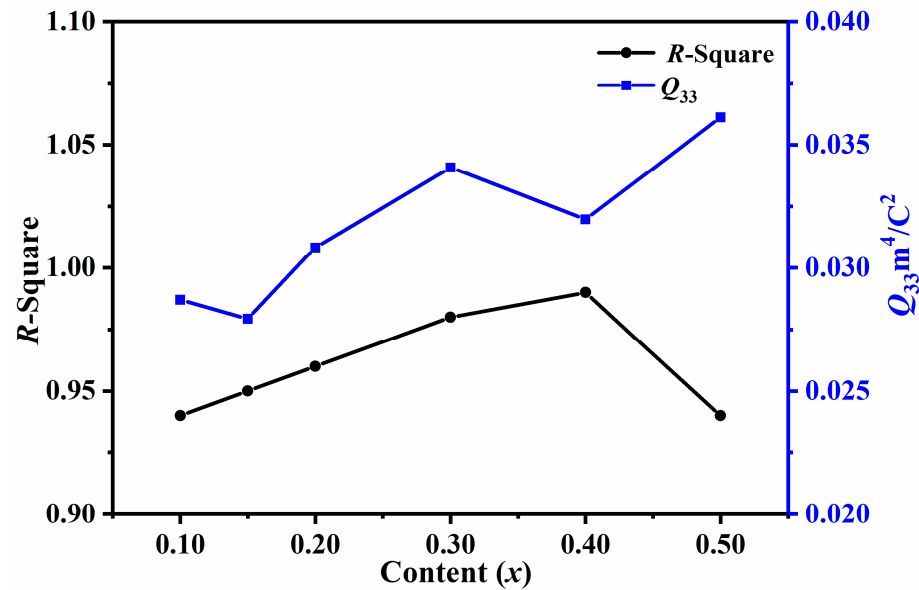


Figure 9. Q_{33} and R as a function of BT-100xST ceramics with different Sr contents.

As can be seen in Figures 8 and 9, the S – P curves of ceramics where $x \leq 0.20$ deviates from the quadratic relation, presenting an obvious hysteresis, which means that the strain is not only based on electrostrictive effect, but also affected by the extrinsic motion of domain walls [39]. The results are in good agreement with the result of the S – E loop. In contrast, S – P curves are well-fitted, based on a quadratic relationship for BT-30ST and BT-40ST ceramics, indicating a favorable electrostriction effect ($R > 0.98$). Furthermore, the Q_{33} of BT-30ST and BT-40ST ceramics are $0.030 \text{ m}^4/\text{C}^2$ and $Q_{33} = 0.034 \text{ m}^4/\text{C}^2$, which are higher than most BNT-based ceramics [41,42].

3.5. Overview

Table 1 summarizes the H_{ys} , Q_{33} and S_{max} properties in the BT-100xST and the recently reported BT-based and other system ceramics. It can be seen that the H_{ys} value is inferior to that of other BT-based and BNT-based piezoelectric ceramics, and the value of Q_{33} is also superior to lead-based and BNT-based piezoelectric ceramics. In addition, the BT-30ST ceramics strain values remain satisfactory. For previously published works, firstly, the giant strain is based on transition from ferroelectric to relaxor phase or ferroelectric to antiferroelectric phase, the result always inevitably accompanied by a large hysteresis in BNT-based ceramics. Secondly, improved Q_{33} and low hysteresis were observed by shifting T_C to around room temperature quickly or designing a relaxor with electrostrictive effect in a lead-based ceramics system; however, the lead material is an unmet demand in practical application. Thirdly, BT-based ceramics can efficaciously suppress hysteresis by chemical modification. Finally, in this work the BT-100xST material was selected and a manner of coexisting phase was designed. The result show that enhanced Q_{33} and suppressive hysteresis.

Table 1. Comparison of Q_{33} , S_{max} , and H_{ys} values of other BT-based, BNT-based and lead-based ceramics.

System	S_{max} (%)	H_{ys} (%)	Q_{33} (m^4/C^2)	Ref.
$Bi_{0.5}(Na_{0.8}K_{0.2})_{0.5}TiO_3$	0.44	60.0	-	[4]
$0.99(Bi_{0.5}Na_{0.4}K_{0.1})TiO_3-0.01(K_xNa_{1-x})NbO_3$	0.46	55.0	-	[5]
$Bi_{0.5}Na_{0.5}TiO_3-Bi_{0.5}K_{0.5}TiO_3-BaZr_{0.05}Ti_{0.95}O_3$	0.12	40	0.0237	[9]
$Bi_4Ti_3O_{12}-Bi_{0.5}(Na_{0.82}K_{0.18})_{0.5}TiO_3$	0.29	23	-	[10]
$Bi_{0.5}(Na_{0.82}K_{0.18})_{0.5}TiO_3-xSn$	0.45	21	0.023	[12]
$Bi_{0.5}Na_{0.5}TiO_3-BaTiO_3-KNbO_3$	0.08	-	0.027	[41]
$Pb(In_{1/2}Nb_{1/2})O_3-Pb(Mg_{1/3}Nb_{2/3})O_3-PbTiO_3$	0.09	5	0.030	[14]
$Bi(Li_{0.5}Nb_{0.5})O_3-Pb(Mg_{1/3}Nb_{2/3})O_3-PbTiO_3$	0.22	7	0.018	[15]
$Pb(Mg_{1/3}Nb_{2/3})O_3-PbTiO_3-Ba(Zn_{1/3}Nb_{2/3})O_3$	0.17	10	0.025	[43]
$BaZr_{0.2}Ti_{0.8}O_3-Ba_{0.7}Ca_{0.3}TiO_3-Ba_{0.7}Sr_{0.3}TiO_3$	0.13	10	-	[19]
$(Ba_{1-y}Ca_y)(Ti_{1-x}Hf_x)O_3$	0.21	12	-	[20]
$(1-x)(Bi_{0.5}Na_{0.5}TiO_3-0.11BaTiO_3)-xBaZr_{0.2}Ti_{0.8}O_3$	0.27	26	0.032	[37]
$BaTiO_3-30SrTiO_3$	0.11	2	0.034	This work

4. Conclusions

In summary, the macroscopic electrostrictive strain of BT-100xST ceramics was analyzed by multi-perspective, including the microstructure, crystal structure, relaxor properties, and ferroelectric properties. A highlight of this investigation is to adjust the composition to promote relaxor behavior appearance with electrostrictive effect, and construct the T—C phase boundary at room temperature. The results demonstrate that the uniform and dense microstructure, along with the coexisting structure of cubic symmetry and tetragonal symmetry, contributes to the superior properties. For the composition of $x = 0.20-0.40$, the frequency shift of T_m and frequency dependence of permittivity as a function of temperature illustrates that the ceramics have canonical relaxor behavior with $\gamma = 1.23-1.36$. Simultaneously, the $P-E$ loops, $S-E$ loops and $I-E$ curves present relaxor behavior characteristics. As a result, an ultra-low hysteresis ($<2\%$) with a high strain ($>0.11\%$) has been successfully acquired at a composition of $x = 0.30$, and accompanied by a superior electrostrictive coefficient Q_{33} ($0.034 m^4/c^2$). Overall, the BT-30ST ceramics would have significant advantages in high-precision ceramic actuators.

Author Contributions: Conceptualization, Y.L. (Yinong Lyu); formal analysis, X.S.; investigation, M.S.; methodology, M.S. and Q.L.; resources, Q.L. and H.Q.; software, H.Q.; supervision, Y.L. (Yunfei Liu) and Y.L. (Yinong Lyu); visualization, X.S.; writing—original draft, M.S.; Writing—review and editing, Y.L. (Yunfei Liu) and Y.L. (Yinong Lyu). All authors have read and agreed to the published version of the manuscript.

Funding: This research received no external funding.

Institutional Review Board Statement: Not applicable.

Informed Consent Statement: Not applicable.

Data Availability Statement: The data presented in this study are available within the article.

Acknowledgments: This work was supported by the Priority Academic Program Development (PAPD) of Jiangsu Higher Education Institutions.

Conflicts of Interest: The authors declare no conflict of interests.

References

- Lu, H.; Liu, L.; Lin, J.; Yang, W.; Zheng, W.; Weng, L.; Zhang, X. Diffuse characteristics and piezoelectric properties of Tb-doped BCZT ceramics with $CaCl_2$ as sintering aid. *Ceram. Int.* **2017**, *43*, 16348–16355. [[CrossRef](#)]
- Wu, Y.; Li, J.; Bai, H.; Hong, Y.; Shi, K.; Zhou, Z.; Guo, R.; Bhalla, A.S. Origin of the dielectric abnormalities and tunable dielectric properties in doped KTN single crystals. *Appl. Phys. Lett.* **2017**, *111*, 242902. [[CrossRef](#)]
- Liu, Q.; Zhang, Y.; Gao, J.; Zhou, Z.; Wang, H.; Wang, K.; Zhang, X.; Li, L.; Li, J. High-performance lead-free piezoelectrics with local structural heterogeneity. *Energ. Environ. Sci.* **2018**, *11*, 3531–3539. [[CrossRef](#)]

4. Hao, J.; Shen, B.; Zhai, J.; Chen, H. Phase transitional behavior and electric field-induced large strain in alkali niobate-modified $\text{Bi}_{0.5}(\text{Na}_{0.80}\text{K}_{0.20})_{0.5}\text{TiO}_3$ lead-free piezoceramics. *J. Appl. Phys.* **2014**, *115*, 034101. [[CrossRef](#)]
5. Hao, J.; Shen, B.; Zhai, J.; Liu, C.; Li, X.; Gao, X. Large Strain Response in $0.99(\text{Bi}_{0.5}\text{Na}_{0.4}\text{K}_{0.1})\text{TiO}_3$ - $0.01(\text{K}_x\text{Na}_{1-x})\text{NbO}_3$ Lead-Free Ceramics Induced by the Change of K/Na Ratio in $(\text{K}_x\text{Na}_{1-x})\text{NbO}_3$. *J. Am. Ceram. Soc.* **2013**, *96*, 3133–3140. [[CrossRef](#)]
6. He, H.; Lu, X.; Li, M.; Wang, Y.; Li, Z.; Lu, Z.; Lu, L. Thermal and compositional driven relaxor ferroelectric behaviours of lead-free $\text{Bi}_{0.5}\text{Na}_{0.5}\text{TiO}_3$ - SrTiO_3 ceramics. *J. Mater. Chem. C* **2020**, *8*, 2411–2418. [[CrossRef](#)]
7. Zhao, J.; Zhang, N.; Quan, Y.; Niu, G.; Ren, W.; Wang, Z.; Zheng, K.; Zhao, Y.; Ye, Z. Evolution of mesoscopic domain structure and macroscopic properties in lead-free $\text{Bi}_{0.5}\text{Na}_{0.5}\text{TiO}_3$ - BaTiO_3 ferroelectric ceramics. *J. Appl. Phys.* **2021**, *129*, 084103. [[CrossRef](#)]
8. Janbua, J.; Niemchareon, S.; Muanghlua, R.; Vittayakorn, N. High Strain Response of the $(1-x)(0.94\text{Bi}_{(0.5)}\text{Na}_{(0.5)}\text{TiO}_{(3)}-0.06\text{BaTiO}_{(3)})$ - $x\text{BaSnO}_{(3)}$ Lead Free Piezoelectric Ceramics System. *Ferroelectrics* **2016**, *490*, 13–22. [[CrossRef](#)]
9. Bai, W.; Chen, D.; Huang, Y.; Zheng, P.; Zhong, J.; Ding, M.; Yuan, Y.; Shen, B.; Zhai, J.; Ji, Z. Temperature-insensitive large strain response with a low hysteresis behavior in BNT-based ceramics. *Ceram. Int.* **2016**, *42*, 7669–7680. [[CrossRef](#)]
10. Fan, P.; Zhang, Y.; Zhang, Q.; Xie, B.; Zhu, Y.; Mawat, M.A.; Ma, W.; Liu, K.; Xiao, J.; Zhang, H. Large strain with low hysteresis in $\text{Bi}_4\text{Ti}_3\text{O}_{12}$ modified $\text{Bi}_{1/2}(\text{Na}_{0.82}\text{K}_{0.18})_{1/2}\text{TiO}_3$ lead-free piezoceramics. *J. Eur. Ceram. Soc.* **2018**, *38*, 4404–4413. [[CrossRef](#)]
11. Liu, X.; Bell, A.J.; Fan, H.; Shi, J. Large Electrostrictive Strain in $(\text{Bi}_{0.5}\text{Na}_{0.5})\text{TiO}_3$ - BaTiO_3 - $(\text{Sr}_{0.7}\text{Bi}_{0.2})\text{TiO}_3$ Solid Solutions. *J. Am. Ceram. Soc.* **2014**, *97*, 848–853.
12. Han, H.; Jo, W.; Kang, J.; Ahn, C.; Kim, I.W.; Ahn, K.; Lee, J. Incipient Piezoelectrics and Electrostriction Behavior in Sn-Doped $\text{Bi}_{1/2}(\text{Na}_{0.82}\text{K}_{0.18})_{1/2}\text{TiO}_3$ Lead-Free Ceramics. *J. Appl. Phys.* **2013**, *113*, 15410215. [[CrossRef](#)]
13. Noblanc, O.; Gaucher, P.; Calvarin, G. Structural and dielectric studies of $\text{Pb}(\text{Mg}_{1/3}\text{Nb}_{2/3})\text{O}_3$ - PbTiO_3 ferroelectric solid solutions around the morphotropic boundary. *J. Appl. Phys.* **1996**, *79*, 4291–4297. [[CrossRef](#)]
14. Qi, X.; Zhao, Y.; Sun, E.; Du, J.; Li, K.; Sun, Y.; Yang, B.; Zhang, R.; Cao, W. Large electrostrictive effect and high energy storage performance of Pr^{3+} doped PIN-PMN-PT multifunctional ceramics in the ergodic relaxor phase. *J. Eur. Ceram. Soc.* **2019**, *39*, 4060–4069. [[CrossRef](#)]
15. Jin, L.; Pang, J.; Luo, W.; Lan, Y.; Du, H.; Yang, S.; Li, F.; Tian, Y.; Wei, X.; Xu, Z.; et al. Phase transition behavior and high electrostrictive strains in $\text{Bi}(\text{Li}_{0.5}\text{Nb}_{0.5})\text{O}_3$ -doped lead magnesium niobate-based solid solutions. *J. Alloys Compd.* **2019**, *806*, 206–214. [[CrossRef](#)]
16. Fu, H.R.; Wang, Y.G.; Guo, H.; Jain, A.; Chen, F.G. Enhancing photostriction in KNN-based ceramics by constructing the morphotropic phase boundary and narrowing the energy band gap. *Ceram. Int.* **2021**, *47*, 10996–11002. [[CrossRef](#)]
17. Shi, P.; Li, T.; Lou, X.; Yu, Z.; Zhu, X.; Zhou, C.; Liu, Q.; He, L.; Zhang, X.; Yang, S. Large electric-field-induced strain and energy storage properties in $\text{Bi}_{0.5}\text{Na}_{0.5}\text{TiO}_3$ - $(0.5\text{Ba}_{(0.7)}\text{Ca}_{(0.3)}\text{TiO}_{(3)})$ - $0.5\text{BaTi}_{(0.8)}\text{Zr}_{(0.2)}\text{O}_{(3)}$ lead-free relaxor ferroelectric ceramics. *J. Alloys Compd.* **2021**, *860*, 206–214.
18. Zhao, C.; Wu, B.; Wu, J. Composition-driven broad phase boundary for optimizing properties and stability in lead-free barium titanate ceramics. *J. Am. Ceram. Soc.* **2019**, *102*, 3477–3487. [[CrossRef](#)]
19. Wu, W.; Ma, J.; Wang, N.; Shi, C.; Chen, K.; Zhu, Y.; Chen, M.; Wu, B. Electrical properties, strain stability and electrostrictive behavior in $0.5\text{BaZr}_{0.2}\text{Ti}_{0.8}\text{O}_3$ - $(0.5-x)\text{Ba}_{0.7}\text{Ca}_{0.3}\text{TiO}_3$ - $x\text{Ba}_{0.7}\text{Sr}_{0.3}\text{TiO}_3$ lead-free ceramics. *J. Alloys Compd.* **2020**, *814*, 152240. [[CrossRef](#)]
20. Zhao, C.; Wu, W.; Wang, H.; Wu, J. Site engineering and polarization characteristics in $(\text{Ba}_{1-y}\text{Ca}_y)(\text{Ti}_{1-x}\text{Hf}_x)\text{O}_3$ lead-free ceramics. *J. Appl. Phys.* **2016**, *119*, 0241082.
21. Zhao, C.; Huang, Y.; Wu, J. Multifunctional barium titanate ceramics via chemical modification tuning phase structure. *Infomat* **2020**, *2*, 1163–1190. [[CrossRef](#)]
22. Zhu, Y. Large electrostrictive properties in lead-free BaTiO_3 - ZnSnO_3 solid solutions. *Appl. Phys. A* **2019**, *125*, 301. [[CrossRef](#)]
23. Maiti, T.; Guo, R.; Bhalla, A.S. Structure-property phase diagram of $\text{BaZr}_x\text{Ti}_{1-x}\text{O}_3$ system. *J. Am. Ceram. Soc.* **2008**, *91*, 1769–1780. [[CrossRef](#)]
24. Teranishi, T.; Kanemoto, R.; Hayashi, H.; Kishimoto, A. Effect of the $(\text{Ba} + \text{Sr})/\text{Ti}$ ratio on the microwave-tunable properties of $\text{Ba}_{0.6}\text{Sr}_{0.4}\text{TiO}_3$ ceramics. *J. Am. Ceram. Soc.* **2017**, *100*, 1037–1043. [[CrossRef](#)]
25. Ying, K.; Hsieh, T. Sintering Behavior, Microstructure, and Dielectric Properties of Nano- $\text{Ba}_{0.7}\text{Sr}_{0.3}\text{TiO}_3$ Ceramics. *Jpn. J. Appl. Phys.* **2008**, *47*, 7947–7952. [[CrossRef](#)]
26. Wu, T.; Pu, Y.; Gao, P.; Liu, D. Influence of Sr/Ba ratio on the energy storage properties and dielectric relaxation behaviors of strontium barium titanate ceramics. *J. Mater. Sci.* **2013**, *24*, 4105–4112. [[CrossRef](#)]
27. Liu, B.; Wang, X.; Zhang, R.; Li, L. Grain size effect and microstructure influence on the energy storage properties of fine-grained BaTiO_3 -based ceramics. *J. Am. Ceram. Soc.* **2017**, *100*, 3599–3607. [[CrossRef](#)]
28. Qiang, H.; Xu, Z. Effects of sintering temperature on the properties of Mn/Y codoped $\text{Ba}_{0.67}\text{Sr}_{0.33}\text{TiO}_3$ ceramics for tunable application. *J. Mater. Sci.* **2015**, *26*, 9063–9066. [[CrossRef](#)]
29. Redhu, P.; Punia, R.; Hooda, A.; Malik, B.P.; Sharma, G.; Sharma, P. Correlation between multifunctional properties of lead free Iron doped BCT perovskite ceramics. *Ceram. Int.* **2020**, *46*, 17495–17507. [[CrossRef](#)]
30. Pavithra, C.; Madhuri, W.; Kiran, S.R. Effects of synthesis and sintering temperature in BCT-BST ceramics. *Mater. Chem. Phys.* **2021**, *258*. [[CrossRef](#)]

31. Jin, L.; Luo, W.; Hou, L.; Tian, Y.; Hu, Q.; Wang, L.; Zhang, L.; Lu, X.; Du, H.; Wei, X.; et al. High electric field-induced strain with ultra-low hysteresis and giant electrostrictive coefficient in barium strontium titanate lead-free ferroelectrics. *J. Eur. Ceram. Soc.* **2019**, *39*, 295–304. [[CrossRef](#)]
32. Wang, T.; Hu, J.; Yang, H.; Jin, L.; Wei, X.; Li, C.; Yan, F.; Lin, Y. Dielectric relaxation and Maxwell–Wagner interface polarization in Nb₂O₅ doped 0.65BiFeO₃-0.35BaTiO₃ ceramics. *J. Appl. Phys.* **2017**, *121*, 084103. [[CrossRef](#)]
33. Kang, F.; Zhang, L.; Huang, B.; Mao, P.; Wang, Z.; Sun, Q.; Wang, J.; Hu, D. Enhanced electromechanical properties of SrTiO₃-BiFeO₃-BaTiO₃ ceramics via relaxor behavior and phase boundary design. *J. Eur. Ceram. Soc.* **2020**, *40*, 1198–1204. [[CrossRef](#)]
34. Wang, J.; Zhang, X.; Zhang, J.; Li, H.; Li, Z. Dielectric and piezoelectric properties of (1-x)Ba_{0.7}Sr_{0.3}TiO₃-xBa_{0.7}Ca_{0.3}TiO₃ perovskites. *J. Phys. Chem. Solids* **2012**, *73*, 957–960. [[CrossRef](#)]
35. Jin, L.; Li, F.; Zhang, S. Decoding the Fingerprint of Ferroelectric Loops: Comprehension of the Material Properties and Structures. *J. Am. Ceram. Soc.* **2014**, *97*, 1–27. [[CrossRef](#)]
36. Prasertpalichat, S.; Khengkhatkan, S.; Siritanon, T.; Jutimoosik, J.; Kidkhunthod, P.; Bongkarn, T.; Patterson, E.A. Comparison of structural, ferroelectric, and piezoelectric properties between A-site and B-site acceptor doped 0.93Bi_{0.5}Na_{0.5}TiO₃-0.07BaTiO₃ lead-free piezoceramics. *J. Eur. Ceram. Soc.* **2021**, *41*, 4116–4128. [[CrossRef](#)]
37. Li, T.; Liu, C.; Ke, X.; Liu, X.; He, L.; Shi, P.; Ren, X.; Wang, Y.; Lou, X. High electrostrictive strain in lead-free relaxors near the morphotropic phase boundary. *Acta Mater.* **2020**, *182*, 39–46. [[CrossRef](#)]
38. Chen, K.; Ma, J.; Wu, J.; Wang, X.; Miao, F.; Huang, Y.; Shi, C.; Wu, W.; Wu, B. Improve piezoelectricity in BaTiO₃-based ceramics with large electrostriction coefficient. *J. Mater. Sci.* **2020**, *31*, 12292–12300. [[CrossRef](#)]
39. Li, F.; Jin, L.; Xu, Z.; Zhang, S. Electrostrictive effect in ferroelectrics: An alternative approach to improve piezoelectricity. *Appl. Phys. Rev.* **2014**, *1*, 11103. [[CrossRef](#)]
40. Jang, S.J.; Uchino, K.; Nomura, S.; Cross, L.E. Electrostrictive behavior of lead magnesium niobate based ceramics dielectric. *Ferroelectric* **1980**, *27*, 31–34. [[CrossRef](#)]
41. Li, J.; Wang, F.; Qin, X.; Xu, M.; Shi, W. Large electrostrictive strain in lead-free Bi_{0.5}Na_{0.5}TiO₃-BaTiO₃-KNbO₃ ceramics. *Appl. Phys. A* **2010**, *104*, 117–122. [[CrossRef](#)]
42. Bai, W.; Li, L.; Wang, W.; Shen, B.; Zhai, J. Phase diagram and electrostrictive effect in BNT-based ceramics. *Solid State Commun.* **2015**, *206*, 22–25. [[CrossRef](#)]
43. Jin, L.; Luo, W.; Jing, R.; Qiao, J.; Pang, J.; Du, H.; Zhang, L.; Hu, Q.; Tian, Y.; Wei, X.; et al. High Dielectric Permittivity and Electrostrictive Strain in a Wide Temperature Range in Relaxor Ferroelectric (1-x)[Pb(Mg_{1/3}Nb_{2/3})O₃-PbTiO₃]-xBa(Zn_{1/3}Nb_{2/3})O₃ Solid Solutions. *Ceram. Int.* **2019**, *45*, 5518–5524. [[CrossRef](#)]